Modal Degeneracy in Thermally Loaded Optical Resonators

Amber L. Bullington,* Brian T. Lantz, Martin M. Fejer, and Robert L. Byer

E. L. Ginzton Laboratory, Stanford University, Stanford, California, USA

**Corresponding author: abull@stanford.edu*

LIGO-P070088-00-Z

We characterize thermally-induced effects in an optical resonator illuminated with high-power laser radiation. From thermoelastic deformation of an optic's surface, we observe degeneracy of higher-order spatial modes with the fundamental mode, power transmission limits, and thermally-induced power fluctuation using a Fabry-Perot ring resonator with calibrated absorption loss. A model used to predict the thermal distortion shows reasonable agreement with results. Predictions for two future upgrades to the Laser Interferometer Gravitational-wave Observatory (LIGO) show that coating absorption should be less than 3.8 ppm and 0.44 ppm for Enhanced and Advanced LIGO Fabry-Perot cavities, respectively, to avoid the first higher-order modal degeneracy.

OCIS codes: 140.0140, 140.4780, 230.5750, 140.6810.

1. Introduction

One method of improving the sensitivity of future gravitational-wave detectors calls for increasing the incident laser power. The planned upgrade to the Laser Interferometer Gravitational-Wave Observatory (LIGO), known as Advanced LIGO, calls for a twenty-fold increase in incident laser power up to 200 W [1]. An interim upgrade to the detector, Enhanced LIGO, utilizes an increase in laser power up to 35 W [2]. LIGO's sensitivity for gravitational-wave detection is limited by shot noise above 250 Hz [1], making increased laser power desirable for detecting gravitational-wave signals above this frequency. However, thermally-induced distortion of interferometer optics from thermal lensing and thermoelastic surface deformation can undermine efforts to improve detector sensitivity. While thermal

lensing can significantly impact the beam coupled into and out of an optical resonator, optical surface deformation alters the eigenmode of the cavity and the modes it may support. In this paper, we focus on thermally-induced surface deformation and its consequences for LIGO.

Thermoelastic deformation of a surface from high circulating power inside an optical resonator may impact the performance of Enhanced and Advanced LIGO. Resonators experiencing the highest thermal deformation include Fabry-Perot cavities in the arms of the Michelson interferometer that comprises LIGO and the ring resonators that provide input-beam spatial and spectral filtering. Thermally-induced surface deformation is dominated by absorption in highly reflecting dielectric coatings of these cavities. While coating absorption of 1 ppm or less is achievable with current coating technology, thermal effects remain a concern for future LIGO interferometers. For example, circulating powers in the Advanced LIGO arm cavities will reach 800 kW.

A Fabry-Perot ring cavity, known as a modecleaner, has been designed with calibrated absorption loss to study the effects of thermal loading in an optical resonator with available laser power. Modecleaners in LIGO filter the input beam to the interferometer at various stages to produce a spatially clean and temporally filtered incident beam. Figure 1(a) shows a schematic of a table-top modecleaner. It consists of optics attached to a glass spacer with drilled openings for the circulating beam to traverse free space. The curved optic is attached to a piezo-electric transducer (PZT) for adjusting the cavity length. All optics have low absorption-loss dielectric coatings. The three-bounce geometry is advantageous for separating the modecleaner's reflected beam from the incident beam to avoid back-reflections and eliminates the need for polarizing optics for Pound-Drever-Hall locking of the cavity to resonance [3]. To achieve a calibrated absorption loss, the substrate of the curved optic, M_3, is made of an infrared-absorbing glass, which absorbs at the operating wavelength of 1064 nm. Light that leaks through the dielectric coating of M_3 is absorbed in a thin layer of the substrate beneath the coating. A low-loss coating on a highly absorbing substrate gives a more effective calibrated absorption loss than a purely lossy coating because of better uniformity and linear absorption [4].

Here we present results of thermally loading modecleaners with a high-power laser. One modecleaner with calibrated absorption loss has M_1 and M_2 made of fused silica and M_3 of an IR absorbing glass. This cavity will be referred to as the lossy modecleaner. Another modecleaner consisting entirely of BK7 glass optics is also tested and is referred to as the low-loss modecleaner. Both modecleaners have the same low-loss dielectric coatings. We start by discussing simplified theory for evaluating the deformation from laser heating, followed by a discussion of experimental results. Finally, predictions for the thermal performance of future LIGO resonators are discussed.

2. Thermally Induced Distortion

In this section we present a simple relation between thermoelastic surface deformation and the power absorbed in an optical coating from an incident Gaussian laser beam. This relation also applies to changes in a resonator's characteristics, namely eigenmode waist size and cavity g-factor product. We then discuss how higher-order mode frequencies vary with absorbed power and how this variation impacts resonator performance.

2.A. Model for Thermoelastic Surface Deformation

Absorption in dielectric coatings and the subsequent deformation of optical surfaces is a major cause of degraded transmission of a Fabry-Perot cavity. By assuming that the local deformation in the vicinity of the beam waist at an optic's surface is spherical, Winkler, et. al. [5] approximate the thermal deformation as a local change in the depth of curvature or sagitta across the incident Gaussian beam diameter. The change in sagitta (δs) of an optic is related to absorbed power (P_{abs}) in its coating via

$$\delta s = \frac{\alpha}{4\pi\kappa} P_{abs} \tag{1}$$

α and κ are the thermal expansion coefficient and the thermal conductivity of the optical substrate, respectively. Absorbed power is determined from circulating power via $P_{abs} = a_c P_{circ}$, where a_c is the coating absorption. P_{circ} is related to the input power, P_{in}, and finesse F via

$$\frac{P_{circ}}{P_{in}} \approx \frac{2T_1}{\pi L} F \tag{2}$$

where T_1 and L are the input-optic transmissivity and total cavity losses, respectively.

For calculation purposes, the ring-resonator geometry of a modecleaner has a two-mirror Fabry-Perot equivalent that consists of a flat mirror spaced half the modecleaner's perimeter, p_m, from M_3 in Figure 1(b). From Winkler et. al. [5], the change in beam radius at M_1 from distortion of M_3 is given by

$$\frac{\delta\omega_1}{\omega_1} = -\frac{\pi}{2\lambda} \frac{\delta s_3}{[g_1 g_2 (1 - g_1 g_2)]^{1/2}} \tag{3}$$

where λ is the wavelength of light, ω_1 the beam radius at M_1, δs_3 the sagittal change at M_3, and g_1 and g_2 are the g-factors ($g = 1 - L/R$) of the two-mirror Fabry-Perot equivalent. A modecleaner has $g_1 = 1$ and $g_2 = 1 - p_m/(2R_{cold})$, where R_{cold} is the undistorted radius of curvature of M_3. The beam-radius change at M_1 from sagittal change δs_1 of M_1 is given by [5]

$$\frac{\delta\omega_1}{\omega_1} = \frac{\pi}{2\lambda} \frac{(1 - 2g_1 g_2)\delta s_1}{[g_1 g_2 (1 - g_1 g_2)]^{1/2}}. \tag{4}$$

For the lossy modecleaner, the small deformation of M_1 and M_2 can be neglected compared to the deformation of lossy optic M_3. Thus, any contribution to the distortion of the eigenmode

waist radius from these optics is neglected. From Eqns. (1) - (4), the thermally altered, 'hot' radius of curvature of an optic is

$$R_{hot} = \frac{\omega_{hot}^2}{2s_{hot}} \tag{5}$$

where $\omega_{hot} = \omega_{cold} + \delta\omega$ and $s_{hot} = s_{cold} + \delta s$. ω_{cold} and s_{cold} represent the undistorted waist size and sagitta of the optic. The thermally-induced change in length of the modecleaner is small compared to the change in radius of curvature of the cavity's optics [6], implying that any change in cavity g-factors may be estimated as a change in radius of curvature alone. For example, the hot g-factor product of the lossy modecleaner is written as

$$g_{hot} = g_1 g_2 = 1 - \frac{p_m}{2R_{hot}} \tag{6}$$

The hot g-factor product becomes important when considering modal frequency spacing of a thermally loaded cavity.

2.B. Higher-Order Mode Spacing

Thermal deformation of resonator optics and the resulting change in g-factor product alter the resonance frequency of all modes supported by a cavity. The resonance frequencies of modes in a Fabry-Perot cavity are given by

$$\varpi_{sq} = \frac{\omega_{sq}}{\Delta\omega_{ax}} = q + \frac{s+1}{\pi}\cos^{-1}(g^{1/2}) \tag{7}$$

where ϖ_{sq} is the frequency of the q^{th} axial mode normalized to the axial mode spacing, $\Delta\omega_{ax}$, s is the mode-index sum, and g is the g-factor product [7]. For a Hermite-Gaussian mode represented by TEM_{mn}, $s = m + n$, where m and n are the number of nodes in the horizontal and vertical directions, respectively. Similarly, $s = 2p + l$ for a Laguerre-Gaussian mode represented by LG_{pl}, where the number of radial and azimuthal nodes are given by p and l, respectively.

The three-bounce geometry of a modecleaner results in an additional π phase shift for higher-order modes with certain symmetry. This additional π phase shift resets their resonance frequency by half the axial mode spacing. For TEM_{mn} modes with m odd and LG_{pl} modes with l even and $l > 0$, the modal resonance is given by

$$\varpi_{s'q} = q + \frac{s'+1}{\pi}\cos^{-1}(g^{1/2}) + \frac{1}{2} \tag{8}$$

where s' indicates the given mode-index sum requires this additional frequency shift.

The change in modal resonance frequency with respect to cavity g-factor product is dependent on the mode-index sum, s. Figure 2 shows a plot of normalized resonance frequency versus g-factor for the TEM_{00} and $TEM_{11,0}$ modes of a modecleaner, showing how the

resonance frequency of $TEM_{11,0}$ changes considerably compared to the fundamental-mode resonance. The choice of $TEM_{11,0}$ will become apparent in section 3. The cold cavity g-factor product of a modecleaner is 0.79, as marked by a vertical line on the plot. Thermally loading a modecleaner increases the cavity's g-factor product, resulting in a potential overlap in resonance of a higher-order mode with the fundamental mode. Figure 2 shows the $TEM_{11,0}$ mode overlapping with the TEM_{00} mode for a hot g-factor product, g_{hot}, of 0.8274. In general, a higher-order mode can become degenerate with the fundamental mode when

$$\varpi_{sq'} - \varpi_{0q} = \frac{s}{\pi}\cos^{-1}(g_{hot}^{1/2}) + (q' - q) = k \tag{9}$$

or

$$\varpi_{s'q'} - \varpi_{0q} = \frac{s'}{\pi}\cos^{-1}(g_{hot}^{1/2}) + \frac{1}{2} + (q' - q) = j \tag{10}$$

where k and j are integers. This modal degeneracy significantly impacts Fabry-Perot cavity transmission with important consequences for gravitational-wave detection as will be discussed in subsequent sections.

3. Thermal Loading Experiment

Figure 3 shows a schematic of the experimental layout for testing the thermal response of a modecleaner. A 30-W Master Oscillator Power Amplifier (MOPA) laser beam is filtered via a modecleaner with finesse of 50 to produce a spatially clean, fundamental mode devoid of unwanted higher-order modal content. This cavity is held at resonance via the Pound-Drever-Hall locking technique by controlling the MOPA's frequency. This beam is subsequently mode-matched into the modecleaner to be tested under thermal load. The thermally loaded modecleaner is also locked to resonance via the Pound-Drever-Hall technique by controlling the length of the cavity. The transmitted beam is then analyzed via an identical modecleaner (mode analyzer) whose length is linearly scanned via the PZT attached to M_3 to analyze the beam's spatial-mode content. The distorted cavity's transmission is also analyzed for power variation via a data acquisition system.

A modecleaner can be tested under differing conditions depending on the polarization of the incident light. S-polarized light experiences an additional π phase shift inside a modecleaner relative to p-polarized light, causing the resonances of the two polarizations to not overlap in frequency. This allows a modecleaner to be locked to one polarization with excellent rejection of the orthogonal polarization [8]. Each polarization also has a different finesse, allowing a modecleaner to be thermally loaded with differing levels of input power depending on the intracavity enhancement of a given input polarization. A modecleaner with p-polarized input light has a finesse of 330, while s-polarized input gives a finesse of 5500.

3.A. Measurements of Thermal Loading in the Lossy Modecleaner

3.A.1. P-Polarized Cavity

With p-polarized light, the incident power to the lossy modecleaner is increased incrementally and the cavity locked to resonance at each step. Figure 4 shows a plot of fundamental-mode content as a function of power absorbed in the IR-absorbing glass substrate of the lossy optic. This is measured by scanning the lossy modecleaner's transmitted beam in the mode-analyzer cavity and noting the coupled fundamental-mode content. The absorbed power is deduced from measurements of the transmitted beam power and coating transmissions. The fundamental-mode content decreases rapidly beyond 40 mW of absorbed power but also dips at specific absorbed powers as the thermal load is increased. The first dip in fundamental-mode transmission occurs at 9 mW of absorbed power, resulting in a 2-% drop in fundamental-mode content. A 7-% dip occurs at 35 mW of absorption. Power coupled to the LG_{23} and $TEM_{11,0}$ modes at 9 mW and 35 mW, respectively, dominates these degradations of the transmitted beam. At absorption levels where specific higher-order mode coupling is not observed, a maximum of 2 % of power is coupled into the TEM_{20} and TEM_{02} modes from the thermally-induced curvature mismatch between the incident and distorted cavity eigenmode. Other higher-order modes are also resolved by the mode analyzer at these absorption levels but contain an insignificant amount of power. For example, the LG_{13} and LG_{33} modes are also measured with the mode analyzer at 9 mW of absorption but contain a negligible amount of power. The same results are observed at 35 mW absorption with small power coupling to the $TEM_{13,0}$ and TEM_{90} modes in addition to the $TEM_{11,0}$ mode. Figure 5(a) shows a CCD camera image of the $TEM_{11,0}$ mode overlapping with the fundamental mode of the lossy modecleaner, while Figure 5(b) gives the $TEM_{11,0}$ mode after filtering via the mode-analyzer modecleaner.

As the absorbed power is raised beyond 40 mW, the lossy modecleaner's transmitted power no longer increases linearly with input power as strong coupling to the LG_{12} mode draws power from the fundamental mode. Figure 5(c) shows the highly distorted transmitted beam at 47 mW of absorption, while Figure 5(d) clearly demonstrates via the mode analyzer that the overlapping mode is LG_{12}. Coupling to other higher-order modes is minimal; the measured LG_{22} mode contains 17× less power than the LG_{12} mode.

At 47 mW of absorption and beyond, steady, locked transmitted power from the lossy modecleaner is no longer achieved. A thermally dependent, periodic-power fluctuation causes the transmitted power to vary by as much as 75 % at frequencies ranging from 14 Hz to 30 Hz. Figure 6 gives a plot of this power fluctuation as a function of time for 47 mW of absorbed power. The depth of the fluctuation increases with absorption while the frequency decreases until the servo can no longer maintain lock with the large power variation. During one thermal cycle, the transmitted mode morphs from TEM_{00} to LG_{12}, indicating that

significant power is coupled into the LG_{12} mode. Since the cavity cannot support higher-order mode resonance at maximum power, the overall transmission of the cavity must decline. As M_3 of the lossy modecleaner cools from the decline in thermal load, power may again build up in the fundamental mode, allowing the cycle to repeat. This thermally-induced variation in transmission represents a thermal limit for a Fabry-Perot cavity for gravitational-wave detection.

Higher-order mode overlap with the fundamental mode is used to estimate the thermal distortion of a cavity's optics. When a higher-order mode overlaps in frequency with the fundamental mode, the new hot-cavity g-factor product can be deduced. A plot of g-factor product as a function of absorbed power for the modecleaner is given in Figure 7. Absorption where predicted overlap with indicated mode-index sums occur is highlighted on the graph. The particular mode observed experimentally for a given mode-index sum may be governed by numerous factors such as astigmatism, scatter, optic imperfections, etc. For example using equation (10), the q^{th} axial LG_{12} mode with mode-index sum of 4 overlaps with the $q^{th} - 1$ axial fundamental mode when a modecleaner's g-factor product is equal to 0.8536. From this new g-factor product, the hot radius of curvature of the lossy modecleaner's curved optic is calculated to be 1.43 m, implying a 40 % change in curvature from the undistorted curvature of 1 m. A calculation of the absorbed power from this new radius of curvature gives an absorption of 45 mW, which agrees with the measured 44 - 47 mW range of absorbed power where the LG_{12} mode is observed. The maximum curvature change of 40 % implies the size of the cavity eigenmode waist increases by 7 %. This change in eigenmode size alters the overlap between the cavity eigenmode and input mode by about 1% [6,9], implying that higher-order modal degeneracy can degrade beam quality significantly prior to any substantial thermally-induced alteration of the resonator eigenmode. Table 1 summarizes the calculation of absorption from the observed overlapping higher-order modes, the measured absorption, and calculated, thermally distorted radius of curvature of M_3. Disagreements between calculated and measured absorption may arise from a thermally-dependent resonance frequency shift. An, et. al. [10] have shown that change in cavity length from thermal expansion of optics causes a shift in the resonance frequency proportional to the intracavity power. Thus, as the cavity's frequency shifts with increasing thermal load, a broader range of absorption allows for overlap between a higher-order and fundamental mode. This thermally-dependent frequency shift gives an estimated 8× broader frequency range of overlap compared to the cold-cavity linewidth when coupling to the LG_{12} mode is observed.

3.A.2. S-Polarized Cavity

When the lossy modecleaner is incrementally locked at increasing input power with s-polarized input light, higher-order modal degeneracy is much stronger and occurs at a lower absorption threshold than in the low-finesse case. The first observed modal degeneracy couples 4 % of fundamental-mode power to a $TEM_{9,21}$ mode at 4.25 mW of absorbed power. Observing a mode with index sum of 30 is plausible since the absorption threshold for coupling to these modes is predicted to be near 2.5 mW, as seen in Figure 7. The modecleaner aperture diameter is 13× larger than the beam diameter, resulting in low diffraction loss for large-order modes. As the thermal load is increased, strong coupling to multiple higher-order modes rapidly degrades the fundamental-mode transmission. Fundamental-mode content drops to as low as 57 % at 12 mW of absorbed power. Figure 8 shows a zoomed image of the mode spectrum transmitted by the mode analyzer when scanned with the lossy modecleaner's transmission at a thermal load of 10 mW. Coupling to multiple higher-order modes is apparent with strong coupling to one mode spaced closely to the fundamental mode. This strongly coupled higher-order mode is LG_{15}. This mode has a predicted overlap absorption of 14 mW as seen from its mode-index sum of 7 in Figure 7, which is reasonable when compared to the 10 mW of absorption observed in the experiment. Strong coupling to higher-order modes that overlap with the fundamental mode may be explained by the higher finesse for s- than for p-polarization. From equation (2), the intracavity power gain for s-polarization is 1200, while for p-polarization it is 105. Thus, any higher-order mode degenerate with the fundamental mode sees a power enhancement nearly 12× larger for s-polarization versus p-polarization in a modecleaner. The thermally dependent shift in frequency from thermal expansion of cavity optics also plays a role in the overlap of higher-order modes with the fundamental mode [10]. For example, the resonant frequency shift at 12 mW of absorbed power causes the frequency overlap range of higher-order modes with the fundamental mode to increase by a factor of 25 when compared to the cold cavity linewidth.

3.B. Measurements of Thermal Loading in the Low-Loss Modecleaner

To test a cavity without a lossy optic, the low-loss modecleaner with BK7-substrate optics is tested in s-polarization with the same method as the lossy modecleaner. Transmission increases linearly with input power until 20 mW of absorption in the cavity is reached. Beyond 20 mW, higher-order modal degeneracy rapidly degrades the beam quality. Degenerate higher-order modes also occur at absorptions well below the maximum. The first overlap occurs at 5.1 mW of absorbed power with another overlap at 10 mW of absorption. The large number of nodes in the higher-order modes observed at these absorbed powers make their identification difficult. Based on predictions of modal degeneracy as a function of absorbed power, the $TEM_{0,27}$ and $TEM_{17,0}$ modes are degenerate for 7.1 mW and 9.4 mW absorption,

respectively. These degeneracies are calculated from equations (9) and (10) for the low-loss modecleaner and match well with those observed in the experiment. For p-polarized input, the low-loss modecleaner begins to show some higher-order mode coupling at 5.1 mW of absorption, which is at the maximum available input power. From these results, the higher-order modal degeneracy is not limited to the characteristics of the lossy modecleaner, and this effect should be predictable for any resonator configuration.

4. Predictions for Future LIGO Resonators

Since a weak gravitational-wave signal is detected via the resonant fundamental mode of LIGO, higher-order modal degeneracy caused by thermal loading may have detrimental effects on the performance of the interferometer. Resonators experiencing high circulating powers that may undergo significant thermoelastic surface deformation from coating absorption include the modecleaners and Fabry-Perot light-storage arm cavities for Enhanced and Advanced LIGO. To predict the occurrence of higher-order modal degeneracy with the fundamental mode, new, hot-cavity g-factors are calculated for the maximum thermal load. The new g-factor product is utilized in equations (9) and (10) to find the modes degenerate with the fundamental mode. The coating absorption is assumed to be the same for all resonator optics.

4.A. Modecleaners for Enhanced and Advanced LIGO

Modecleaners are employed in two locations for filtering the input beam to the interferometer. A table-top modecleaner identical in geometry to the modecleaners used in the thermal loading experiment provides the initial filtering of the high-power laser. A modecleaner with a perimeter of several tens of meters and suspended optics (suspended modecleaner) provides additional spatial and temporal filtering up to roughly 10 MHz for the beam incident to the interferometer [11]. These modecleaners utilize optics with low-loss coatings on fused silica substrates. While the thermal conductivity of fused silica is low, its small thermal expansion coefficient, uniformity and ease of manufacture in large diameter make it a desirable substrate material for LIGO.

For coating absorption loss of 1 ppm, the table-top modecleaners for Enhanced and Advanced LIGO are predicted to show insufficient thermoelastic deformation to have any degenerate higher-order modes. Coating absorptions of 6 ppm and 8.5 ppm for the Enhanced and Advanced LIGO table-top modecleaners, respectively, are needed to reach the first modal overlaps that have mode-index sums of 10, 20, 30, etc. However, the suspended modecleaners for Enhanced and Advanced LIGO show sufficient thermal loading for 1 ppm coating absorption to experience some modal degeneracy. Table 2 lists the properties of these modecleaners as well as their modal overlaps. The degenerate higher-order modes have large order

(11 and higher), indicating that a proper choice of aperture may suppress coupling to these modes. The aperture formed by the mirror itself compared with the beam size is insufficient to suppress higher-order modes. Coating absorptions for each Enhanced and Advanced LIGO modecleaner must reach 4.7 ppm and 4.2 ppm, respectively, to reach a degenerate mode-index sum that is less than 10. Thus, with coating absorptions at 1 ppm or less and proper aperturing, higher-order mode coupling may be avoidable in the these cavities.

4.B. Fabry-Perot Arm Cavities for Enhanced and Advanced LIGO

To increase interaction time with a gravitational wave, LIGO has 4-km Fabry-Perot cavities in each arm of its Michelson configuration [1]. These resonators experience the highest circulating power of any cavity employed in LIGO. For 25 W incident on the interferometer for Enhanced LIGO, the arm cavities experience a maximum circulating power of 100 kW [12]. For Advanced LIGO with 125 W incident on the interferometer, the arm cavities will be subjected to 800 kW of circulating power [13]. A list of arm cavity parameters is given in table 3.

Low coating absorption is important for minimizing higher-order mode overlap. Figures 9 and 10 show plots of cavity g-factor product versus the coating absorption of a single optic for both the Enhanced and Advanced LIGO arm cavities. Mode-index sums for degenerate higher-order modes are marked along the plots. Vertical lines denote the maximum thermal load experienced for a given coating absorption, indicating that small variations in coating absorption can greatly affect the number of degenerate higher-order modes seen with increasing intracavity power. Diffraction loss also plays a roll in the higher-order modes an arm cavity may support. The maximum mode-index sum supported by a resonator can be approximated by $s_{max} \approx (a/\omega)^2$, where a and ω are the optic and beam radii, respectively [7]. $s_{max} = 8$ for both Enhanced and Advanced LIGO.

From Figure 9, an Enhanced LIGO arm cavity is likely to show modal degeneracy at 800 mW of total coating absorption for an index sum of 7. To avoid this modal overlap, coating absorption should be less than 3.8 ppm. From Figure 10, an Advanced LIGO arm cavity may show modal degeneracy with modes having index sums less than 8 at 706 mW, 1.76 W, and 3.48 W total coating absorption for mode-index sums of 7, 6 and 5, respectively. Since an Advanced LIGO arm cavity approaches a confocal resonator as it is heated, its g-factor product will decrease until the mirror radii of curvature equals the length of the cavity. This arm cavity is unlikely to become confocal thermally since the mirror radii of curvature must change by nearly a factor of two. Note that the cold Advanced LIGO arm cavity is nearly degenerate with mode-index sum of 8, needing only 14 mW of total coating absorption for degeneracy, making this overlap unavoidable as power is increased. A coating absorption of less than 0.44 ppm must be obtained to avoid the thermally-induced modal overlap at

mode-index sum of 7, which may push the absorption-loss limit of available dielectric-coating technology. Furthermore, coating inhomogeneities from dust or other contamination may also induce higher-order modal degeneracy at thresholds lower than those predicted for uniform coating absorption. Coating uniformity will be most critical for the arm cavities of Advanced LIGO.

5. Conclusion

We have shown that thermoelastic deformation from absorbed power in an optical coating may induce higher-order modal degeneracy with the fundamental mode of a resonator. Using a modecleaner with calibrated absorption loss, higher-order mode coupling showed agreement with theoretical values for given absorption. A thermally-dependent power fluctuation was observed under strong thermal loading. Finesse also governed the strength of the higher-order mode coupling, resulting in greater higher-order mode coupling for higher finesse. A thermally loaded low-loss modecleaner demonstrated that modal degeneracy predictions should be possible for any resonator configuration.

Based on modeling of the thermally-induced mode overlaps observed experimentally, predictions were made for modal degeneracy in future upgrades to LIGO. Suspended modecleaners for Enhanced and Advanced LIGO may avoid modal degeneracy with proper aperturing for higher-order modes with coating absorption of 1 ppm. While aperture size may suppress some higher order modes in the arm cavities, modal degeneracy is predicted in Enhanced LIGO for coating absorption exceeding 3.8 ppm and in Advanced LIGO for absorption greater than 0.44 ppm.

An interferometer that employs gratings in an all-reflective topology may use substrates with better thermal properties (e.g. silicon) than those only available for transmission at the operating wavelength of 1064 nm [14]. For example, the ratio of change in sagitta, δs, of fused silica to silicon is 20, implying that 20$\times$ the power may be absorbed in a silicon substrate than a fused silica one for the same thermoelastic deformation. An all-reflective Sagnac interferometer for gravitational-wave detection has been demonstrated using silicon optics [15]. Furthermore, silicon may be cooled to cryogenic temperatures where its thermal expansion coefficient approaches zero at 18 K and 120 K [16], helping to avoid any modal degeneracy induced by thermal distortion. Alternative substrates and interferometer topology may be necessary to avoid thermal effects when considering gravitational-wave detectors beyond Advanced LIGO.

Acknowledgements

This work was supported by the National Science Foundation under grant PHY-05-02641. The authors thank members of the LIGO Scientific Collaboration for insightful discussion.

A. Bullington also acknowledges support from a National Science Foundation Graduate Research Fellowship.

References

1. P. Fritschel, "The second generation LIGO interferometers," in *Proceedings of Astrophysical Sources for Ground-Based Gravitational Wave Detectors*, J. M. Centrella, ed., pp. 15–23 (American Institute of Physics, 2001).
2. R. Adhikari, P. Fritschel, and S. Waldman, "Enhanced LIGO," http://www.ligo.caltech.edu/docs/T/T060156-01.pdf.
3. R. W. P. Drever, J. L. Hall, F. V. Kowalski, J. Hough, G. M. Ford, A. J. Munley, and H. Ward, "Laser phase and frequency stabilization using an optical resonator," Appl. Phys. B: Photophys. Laser Chem. **31**, 97–105 (1983).
4. C. Janke, "Thermal loading of optical components in interferometric systems," (2001). Presented at the LIGO Scientific Collaboration Conference.
5. W. Winkler, K. Danzmann, A. Rudiger, and R. Schilling, "Heating by optical absorption and the performance of interferometric gravitational-wave detectors," Phys. Rev. A **44**, 7022–7036 (1991).
6. N. Uehara, E. K. Gustafson, M. M. Fejer, and R. L. Byer, "Modeling of efficient mode matching and thermal-lensing effect on a laser-beam coupling into a mode-cleaner cavity," Proc. SPIE **2989**, 57–98 (1997).
7. A. E. Siegman, *Lasers* (University Science, Mill Valley, Calif., 1986). Errata URL: http://www-ee.stanford.edu/siegman/lasersbookerrata.txt.
8. S. Saraf, R. L. Byer, and P. J. King, "High-extinction-ratio resonant cavity polarizer for quantum-optics measurements," Appl. Opt. **46**, 3850–3855 (2007).
9. H. Kogelnik, "Coupling and Conversion Coefficients for Optical Modes," in *Proceedings of the Symposium on Quasi-Optics*, pp. 333–347 (Polytechnic Press, Brooklyn, USA, 1964).
10. K. An, B. A. Sones, C. Fang-Yen, R. R. Dasari, and M. S. Feld, "Optical bistability induced by mirror absorption: measurement of absorption coefficients at the sub-ppm level," Opt. Lett. **22**, 1433–1435 (1997).
11. D. Tanner, Department of Physics, University of Florida, P.O. Box 118440, Gainesville, FL, 32611 (personal communication, 2007).
12. R. Adhikari, Department of Physics, California Institute of Technology, Physics Department 103-33, Pasadena, CA, 91125 (personal communication, 2007).
13. P. Fritschel, "Advanced LIGO interferometer parameters," http://emvogil-3.mit.edu/ pf/advligo/SYS/ALparameters.htm.

14. K. X. Sun and R. L. Byer, "All-reflective Michelson, Sagnac, and Fabry-Perot interferometers based on grating beam splitters," Opt. Lett. **23**, 567–569 (1998).
15. P. Beyersdorf, "Results from the Stanford 10 m Sagnac interferometer," in *Proceedings of the* 4^{th} *Edoardo Amaldi Conference on Gravitation Waves*, vol. 19, pp. 1585–1589 (Classical and Quantum Gravity, 2001).
16. S. Rowan, J. Hough, and D. R. M. Crooks, "Thermal noise and material issues for gravitational wave detectors," Phys. Lett. A **347**, 25–32 (2005).

List of Figures

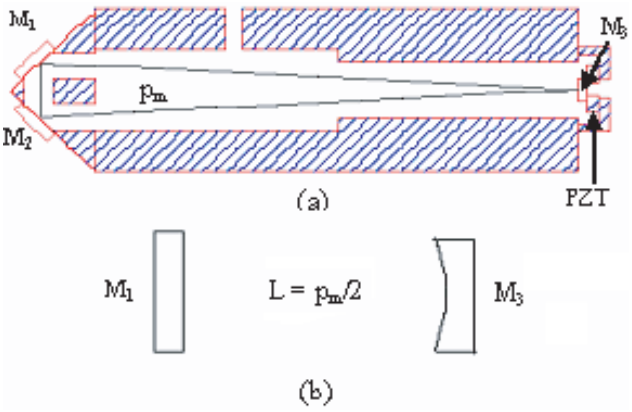

Fig. 1. (a) A schematic of a Fabry-Perot ring resonator (modecleaner) is shown. M_1 and M_2 are 1 inch in diameter, and M_3, attached to a piezoelectric transducer (PZT), is 0.5 inch in diameter with a 1-m radius of curvature. Round-trip perimeter, p_m, is 42 cm. (b) Two-mirror Fabry-Perot equivalent to a modecleaner for thermal analysis is shown.

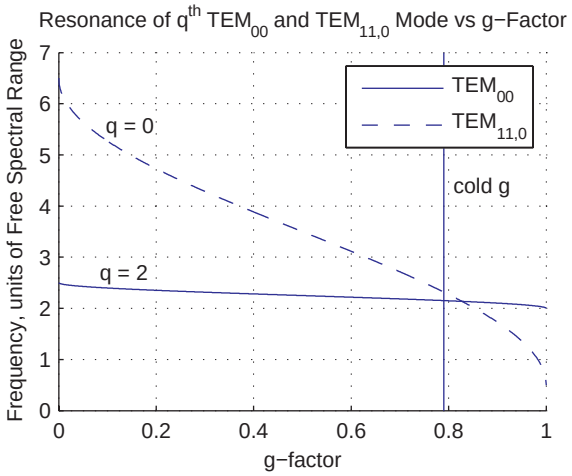

Fig. 2. Normalized modal resonance frequency is plotted versus g-factor product for the q^{th} axial $TEM_{11,0}$ and $q^{th} + 2$ TEM_{00} modes of a modecleaner. A vertical line at g = 0.79 indicates a modecleaner's undistorted cavity g-factor product. The resonance frequency of $TEM_{11,0}$ changes significantly compared to TEM_{00}, overlapping in resonance with the fundamental mode for g = 0.8274.

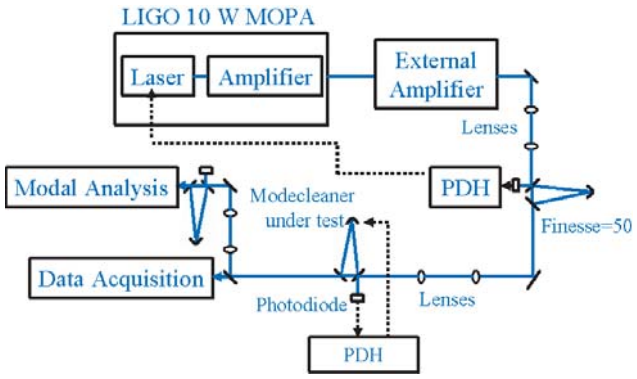

Fig. 3. The experimental layout for testing a Fabry-Perot ring resonator (modecleaner) under thermal load is shown. A finesse-of-50 modecleaner filters the 30-W Master Oscillator Power Amplifier system via the Pound-Drever-Hall (PDH) locking technique to provide a spatially clean input beam to the cavity to be tested under thermal load. Output from the thermally loaded modecleaner is subsequently transmitted to an identical modecleaner for analyzing modal content. The distorted transmission is also analyzed for power variation via a data acquisition system.

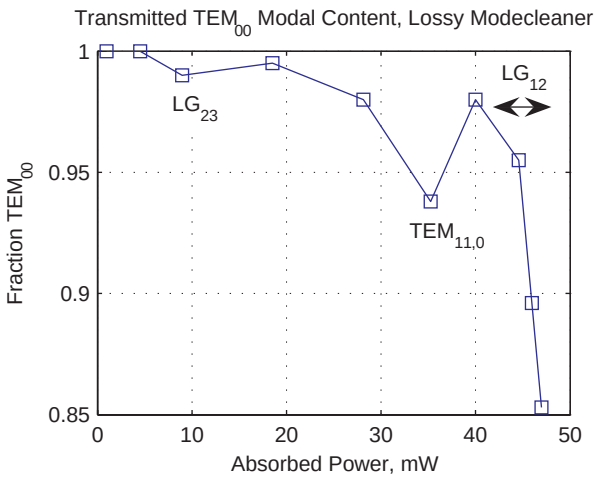

Fig. 4. Transmitted TEM_{00} modal content is plotted as a function of absorbed power in the lossy modecleaner. Beyond 40 mW of absorbed power, the fundamental-mode content rolls off sharply from coupling to the LG_{12} mode. Additional higher-order mode coupling is observed at 9 mW and 35 mW of absorbed power, where power is coupled into the LG_{23} and $TEM_{11,0}$ modes, respectively.

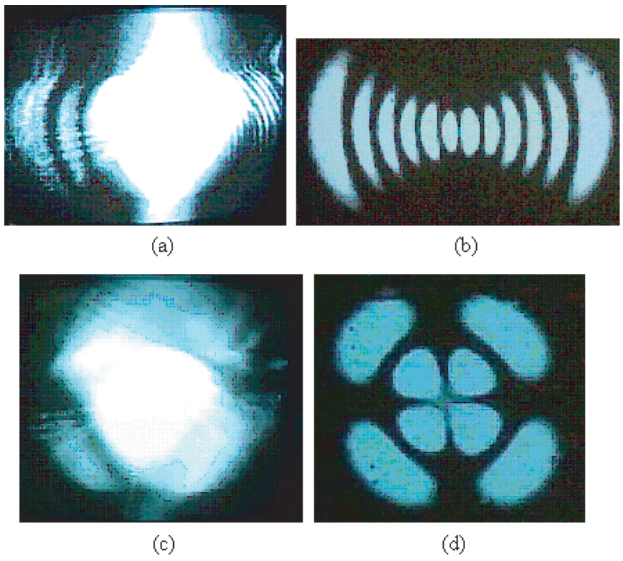

Fig. 5. CCD image (a) shows the transmitted beam of the lossy modecleaner containing both TEM_{00} and $TEM_{11,0}$ higher-order modes at 35 mW of absorbed power. The CCD camera is allowed to be slightly saturated to fully resolve the higher-order mode. Image (b) shows the $TEM_{11,0}$ mode when the beam from image (a) is filtered via an additional, identical modecleaner (mode analyzer). Images (c) and (d) show the lossy modecleaner's transmitted beam and resultant filtering via the mode-analyzer cavity at 47 mW of absorbed power.

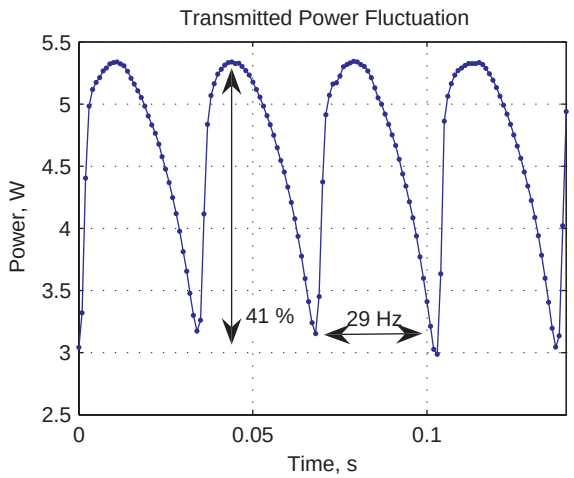

Fig. 6. A periodic fluctuation in power dependent on thermal load is shown. For 47 mW of absorbed power, the transmission of the lossy modecleaner fluctuates at a frequency of 29 Hz with a fluctuation depth of 41%.

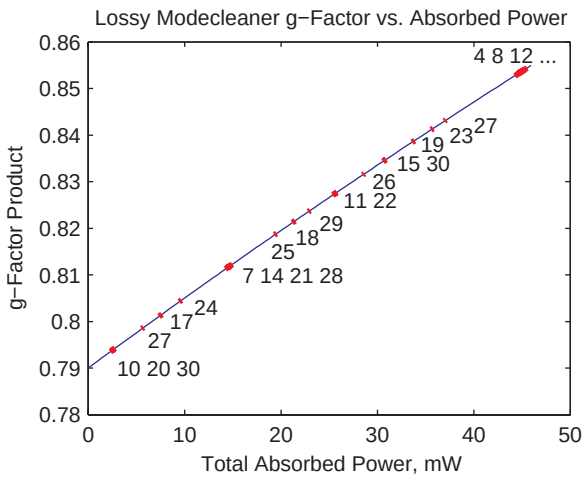

Fig. 7. The lossy modecleaner's g-factor product is plotted as a function of absorbed power. Predicted mode overlaps are highlighted along the curve with the appropriate mode-index sums (defined as $m + n$ for TEM_{mn} modes and $2p+l$ for LG_{pl} modes). The range of each overlap is estimated from the change in g-factor product needed for a higher-order mode to overlap within the modecleaner's undistorted Full Width at Half Maximum (FWHM).

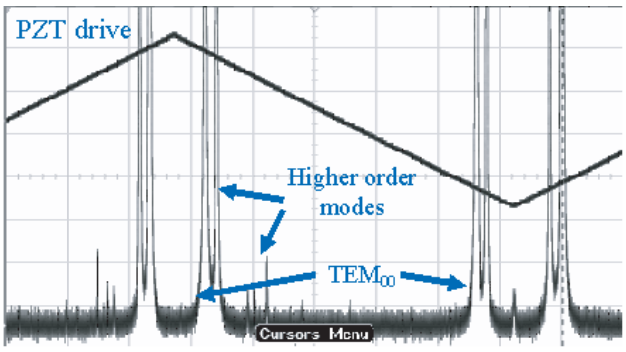

Fig. 8. A zoom-in of an oscilloscope trace of the transmission of the mode analyzer cavity is shown when the lossy modecleaner has 10 mW absorption with s-polarization. The triangle wave gives the drive to the mode analyzer's PZT. Coupling to multiple higher-order modes is visible with strong coupling to one mode closely spaced to the fundamental mode.

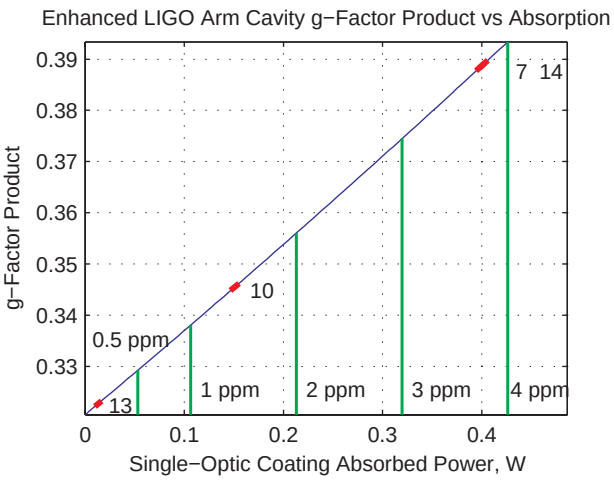

Fig. 9. The g-factor product versus coating absorption of a single optic is plotted for an Enhanced LIGO arm cavity. Predicted mode-index sums giving higher-order modal degeneracy are highlighted along the curve similar to that shown in Figure 7. Vertical lines mark the maximum absorbed power for a given coating absorption. The greater the absorption, the larger the number of possible degenerate higher-order modes.

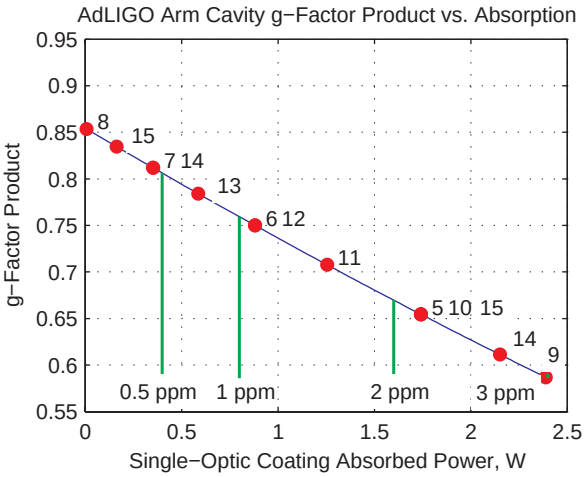

Fig. 10. Advanced LIGO arm cavity g-factor product versus coating absorption of a single optic is shown similar to Figure 9. Predicted degenerate mode-index sums are highlighted and vertical lines mark maximum absorbed power for a given coating absorption. Advanced LIGO arm cavities become more susceptible to modal degeneracy at low coating absorption because of high circulating power.

Table 1. Comparison of Measured and Calculated Absorption in the Lossy Modecleaner for Each Observed Higher-Order Mode with Estimated Hot Radius of Curvature (ROC)

Observed Mode	LG_{23}	$TEM_{11,0}$	LG_{12}
Calculated Absorption (mW)	14.6	25.6	45
Measured Absorption (mW)	9	35	44-47[a]
M_3 Hot ROC (m)	1.11	1.22	1.43

[a] LG_{12} mode is observed over a range of absorbed powers.

Table 2. Suspended Modecleaner Properties and Degenerate Higher-Order Modes for 1 ppm Coating Absorption Loss

Suspended Modecleaner	Perimeter (m)	M_3 Radius of Curvature (m)	Finesse	Maximum Circulating Power (kW)	Total Coating Absorption[a] (mW)	Degenerate Mode-Index Sum(s)
Enhanced LIGO	24.48	17.25	1700	15	23.5	11 and 22
Advanced LIGO	33.33	25.95	500	24	11.5 / 60	22 / 17

[a] Single-optic coating absorption ×3.

Table 3. Properties of Fabry-Perot Arm Cavities for Enhanced and Advanced LIGO

	Enhanced LIGO[a]	Advanced LIGO[b]
Radius of Curvature (m), M_1	13910	2076
Radius of Curvature (m), M_2	7260	2076
Cavity Length (m)	3995	3995
Optic Radius (cm)	12.5	17
Beam Radius at M_1 (cm)	3.61	5.96
Beam Radius at M_2 (cm)	4.55	5.96
Finesse	220	1257

[a] Enhanced LIGO arm cavity properties are from the LIGO site in Hanford, WA.

[b] Advanced LIGO data are based on the latest design information [13].